

Light Axial Vectors, Nuclear Transitions, and the ${}^8\text{Be}$ Anomaly

Jonathan Kozaczuk^(a,b), David E. Morrissey^(b), and S. R. Stroberg^(b,c)

(a) *Amherst Center for Fundamental Interactions, Department of Physics,
University of Massachusetts, Amherst, MA 01003, USA*

(b) *TRIUMF, 4004 Wesbrook Mall, Vancouver, BC V6T 2A3, Canada*

(c) *Reed College, 3203 SE Woodstock Blvd, Portland, OR 97202, USA*

email: kozaczuk@umass.edu, dmorri@triumf.ca, sstroberg@triumf.ca

July 6, 2017

Abstract

New hidden particles could potentially be emitted and discovered in rare nuclear transitions. In this work we investigate the production of hidden vector bosons with primarily axial couplings to light quarks in nuclear transitions, and we apply our results to the recent anomaly seen in ${}^8\text{Be}$ decays. The relevant matrix elements for ${}^8\text{Be}^*(1^+) \rightarrow {}^8\text{Be}(0^+)$ transitions are calculated using *ab initio* methods with inter-nucleon forces derived from chiral effective field theory and the in-medium similarity renormalization group. We find that the emission of a light axial vector with mass $m_X \simeq 17$ MeV can account for the anomaly seen in the $1^+ \rightarrow 0^+$ isoscalar transition together with the absence of a significant anomaly in the corresponding isovector transition. We also show that such an axial vector can be derived from an anomaly-free ultraviolet-complete theory that is consistent with current experimental data.

1 Introduction

The search for new forces has been a longstanding pursuit of subatomic physics research [1, 2]. New force carriers that couple significantly to the Standard Model (SM) have been searched for directly at high energy colliders such as the LHC [3, 4, 5, 6] and tested indirectly through high-precision measurements [7], and they must have masses well above the electroweak scale to be consistent with these data. Exotic force carriers with masses below the electroweak scale are also allowed by current experiments if they are *hidden*, coupling very weakly to SM matter [8, 9, 10, 11]. The most sensitive searches for light hidden states are typically lower-energy collider experiments with a very high intensity of collisions [11, 12, 13, 14, 15, 16]. Experiments of very high precision are also competitive in terms of current limits and future discovery prospects [10, 15].

Light vector boson force carriers and other light hidden particles with masses up to a few tens of MeV can also be searched for in rare nuclear decays [17, 18]. Various types of hidden particles can be emitted in such transitions depending on the spin and parity of the initial and final nuclear states. Indeed, significant limits on axions have been derived from precision measurements of ^8Be , ^{14}N , and ^{16}O decays [19, 20, 21]. More recently, the emission of hidden vector bosons by nuclei has received particular attention due to an apparent anomaly seen in measurements of ^8Be transitions [22].

An experiment at the MTA-Atomki facility reports a significant (6.8σ) bump in the distribution of opening angles between energetic electron-positron pairs emitted in isoscalar $^8\text{Be}^*(1^+) \rightarrow ^8\text{Be}(0^+) + e^+e^-$ transitions [22]. No such bump is expected from known nuclear physics, which predicts that this transition arises primarily from internal pair conversion with a smoothly falling distribution of e^+e^- opening angles. Furthermore, no significant excess is seen in the related isovector $^8\text{Be}^{*'}(1^+) \rightarrow ^8\text{Be}(0^+) + e^+e^-$ transition [22]. For future reference, we list the relevant ^8Be states in Table 1, together with their masses, excitation energies, relevant decay widths, and angular momentum (J), parity (P), and approximate isospin (T) quantum numbers [23].

This apparent anomaly in ^8Be transitions can be explained by an additional decay channel to a light vector boson X , $^8\text{Be}^*(1^+) \rightarrow ^8\text{Be}(0^+) + X$, followed by $X \rightarrow e^+e^-$ [22, 24]. To match the kinematic feature seen in e^+e^- opening angles, the new vector should have a mass $m_X \simeq 17$ MeV [22]. This proposal was studied in detail in Refs. [24, 25] for a vector boson with purely *vector* (as opposed to axial) couplings to quarks. These works showed that such an explanation can be consistent with existing experimental constraints provided the new vector is approximately *protophobic* [24], coupling much more weakly to the proton than to the neutron. Further related investigations and interpretations of the excess have appeared as well [26, 27, 28, 29, 30, 31, 32, 33, 34, 35].

In this work we investigate whether a new vector boson with primarily *axial* couplings to quarks can account for the ^8Be anomaly. This possibility was suggested in Refs. [24, 25], but it was not pursued systematically due to the difficulty of computing the corresponding nuclear matrix elements. We confront this challenge head on, and apply state-of-the-art *ab initio* nuclear theory methods to derive a controlled estimate of the relevant nuclear physics

State	m (MeV)	ΔE (MeV)	Γ (keV)	Γ_γ (eV)	J_T^P
${}^8\text{Be}$	7454.85	0	–	–	0_0^+
${}^8\text{Be}^*$	7473.00	18.15	138	1.9	1_0^+
${}^8\text{Be}^{*'} $	7472.49	17.64	10.7	15	1_1^+

Table 1: ${}^8\text{Be}$ ground and excited states relevant to the Atomki anomaly [22] together with their mass, excitation energy, total decay width, decay width to ${}^8\text{Be} + \gamma$, spin (J), parity (P), and approximate isospin (T) assignments [23, 24].

quantities. We then apply our results to the ${}^8\text{Be}$ anomaly to determine whether a hidden axial vector can provide a viable explanation.

The outline of this paper is as follows. After this introduction, we adapt the formalism of electromagnetic and weak nuclear decays to general nuclear decays with the emission of a light hidden particle in Section 2, and we apply it to the ${}^8\text{Be}$ system with a light vector with axial couplings to quarks. In Section 3 we present our nuclear physics calculation of the transition matrix elements relevant to the ${}^8\text{Be}$ anomaly. These results are then applied to study an axial vector interpretation of the anomaly in Section 4. A comparison of this interpretation with other limits on light axial vectors are studied in Section 5. We comment on UV completions with light axial vectors consistent with the ${}^8\text{Be}$ anomaly in Section 6. Finally, Section 7 is reserved for our conclusions.

2 Nuclear Decay Rates to a Massive Vector

In this section we adapt the formalism of electromagnetic and weak nuclear decays to general nuclear transitions in which a light (but massive) vector boson is emitted, and we derive a general expression for the corresponding decay rate in terms of the underlying nucleon current coupling. Next, we specialize to a light vector with axial couplings to quarks and obtain the relevant nucleon-level currents and a simplified expression for the transition matrix elements. These results are then applied to ${}^8\text{Be}^*(1^+) \rightarrow {}^8\text{Be}(0^+)$ transitions.

2.1 General Formalism for Nuclear Decays

Consider a massive vector boson X that couples to hadrons in the SM through the current

$$\mathcal{H}_{int} \supset \mathcal{J}_\mu X^\mu . \quad (1)$$

This interaction can potentially lead to nuclear decays of the form $|i\rangle \rightarrow |f\rangle + X$, provided the vector is light enough. At leading order in the interaction of Eq. (1), the corresponding (Schrödinger picture) transition matrix element is

$$\mathcal{M} = \int d^3x \langle f | \mathcal{J}_\mu e_a^{\mu*} e^{-i\vec{k}\cdot\vec{x}} | i \rangle , \quad (2)$$

where ϵ_a^μ is the polarization vector of the outgoing vector boson with 3-momentum \vec{k} and polarization state a .

To evaluate the nuclear matrix element, it is conventional to expand it in terms of spherical tensor operators [36, 37]. If the initial state is unpolarized, the quantization axis for angular momentum can be chosen parallel to $\vec{k} \rightarrow k \hat{z}$. In this case, the three polarization vectors can be taken to be

$$\epsilon_0^\mu = \frac{1}{m_X}(k, 0, 0, E_k), \quad \epsilon_{\pm 1}^\mu = \mp \frac{1}{\sqrt{2}}(0, 1, \pm i, 0). \quad (3)$$

Defining the spherical basis $\hat{e}_0 = \hat{z}$ and $\hat{e}_{\pm 1} = \mp(\hat{x} \pm i\hat{y})/\sqrt{2}$, we have

$$\vec{\epsilon}_a^* = \sum_\lambda (\vec{\epsilon}_a^* \cdot \hat{e}_\lambda) \hat{e}_\lambda^* \equiv \sum_\lambda (\epsilon_a^*)_\lambda \hat{e}_\lambda^* \quad (4)$$

with

$$(\epsilon_a^*)_0 = \frac{E_k}{m_X} \delta_{a0}, \quad (\epsilon_a^*)_{\pm 1} = \delta_{a\pm 1}, \quad \epsilon_a^{0*} = \frac{k}{m_X} \delta_{a0}. \quad (5)$$

The operators $\hat{e}_\lambda^* e^{-ikz}$ can be expanded in a spherical vector basis to give [37]

$$\begin{aligned} \mathcal{M} = -\langle f | & \left(\sum_{J \geq 1} (-i)^J \sqrt{2\pi(2J+1)} \sum_{\lambda=\pm 1} (\epsilon_a^*)_\lambda [\lambda \mathcal{T}_{J,-\lambda}^{mag}(k) + \mathcal{T}_{J,-\lambda}^{el}(k)] \right. \\ & \left. + \sum_{J \geq 0} (-i)^J \sqrt{4\pi(2J+1)} [(\epsilon_a^*)_0 \mathcal{L}_{J0}(k) - \epsilon_a^{0*} \mathcal{M}_{J0}] \right) |i\rangle, \end{aligned} \quad (6)$$

where

$$\mathcal{M}_{JM}(k) = \int d^3x j_J(kr) Y_{JM}(\Omega) \mathcal{J}^0(\vec{x}) \quad (7)$$

$$\mathcal{L}_{JM}(k) = \frac{i}{k} \int d^3x \vec{\nabla} [j_J(kr) Y_{JM}(\Omega)] \cdot \vec{\mathcal{J}}(\vec{x}) \quad (8)$$

$$\mathcal{T}_{JM}^{el}(k) = \frac{1}{k} \int d^3x \vec{\nabla} \times [j_J(kr) \hat{\mathcal{Y}}_{J,J1}^M(\Omega)] \cdot \vec{\mathcal{J}}(\vec{x}) \quad (9)$$

$$\mathcal{T}_{JM}^{mag}(k) = \int d^3x [j_J(kr) \hat{\mathcal{Y}}_{J,J1}^M(\Omega)] \cdot \vec{\mathcal{J}}(\vec{x}). \quad (10)$$

The quantities $\hat{\mathcal{Y}}_{J,\ell 1}^M$ are the *vector spherical harmonics*, defined according to [36, 37]

$$\hat{\mathcal{Y}}_{J,\ell 1}^M(\Omega) = \sum_{m,\lambda} \langle \ell m; 1\lambda | \ell 1; JM \rangle Y_{\ell m}(\Omega) \hat{e}_\lambda. \quad (11)$$

The utility of the form of Eq. (6) is that the operators appearing in the expansion, Eqs. (7–10), can be shown to be irreducible spherical tensors of degree JM (for current operators of a reasonable form) [37]. This allows for the application of selection rules based on angular

momentum and parity. In particular, for any such operator \mathcal{O}_{JM} , the Wigner-Eckart theorem gives

$$\langle J_f, M_f | \mathcal{O}_{JM} | J_i, M_i \rangle = \frac{(-1)^{J_i - M_i}}{\sqrt{2J + 1}} \langle J_f, M_f; J_i, -M_i | J_f J_i; J, M \rangle \langle J_f || \mathcal{O}_{JM} || J_i \rangle, \quad (12)$$

where the first matrix element refers to Clebsch-Gordan coefficients and the second is a *reduced matrix element* that is independent of M , M_i , and M_f .

For initial and final nuclear states of the form $|i\rangle = |J_i, M_i\rangle$ and $|f\rangle = |J_f, M_f\rangle$, squaring and summing the matrix element and applying the orthogonality of Clebsch-Gordan coefficients gives

$$\begin{aligned} \frac{1}{2J_i + 1} \sum_{M_i, M_f, a} |\mathcal{M}|^2 &= \frac{4\pi}{2J_i + 1} \left(\sum_{J \geq 1} |\langle J_f || (\lambda \mathcal{T}_J^{mag} + \mathcal{T}_J^{el} || J_i \rangle|^2 \right. \\ &\quad + \sum_{J \geq 0} \left[\left(\frac{E_k}{m_X} \right)^2 |\langle J_f || \mathcal{L}_J || J_i \rangle|^2 + \left(\frac{k}{m_X} \right)^2 |\langle J_f || \mathcal{M}_J || J_i \rangle|^2 \right. \\ &\quad \left. \left. - 2 \frac{k E_k}{m_X^2} \operatorname{Re} \langle J_f || \mathcal{L}_J || J_i \rangle \langle J_f || \mathcal{M}_J || J_i \rangle^* \right] \right). \end{aligned} \quad (13)$$

Note that this expression can also be adapted to decays to a massless vector by setting \mathcal{L}_J and \mathcal{M}_J to zero, and to decays to a scalar by keeping only \mathcal{M}_J non-zero and removing the factor of $(k/m_X)^2$ from the remaining term.

The final unpolarized decay rate for $|i\rangle \rightarrow |f\rangle + X$ (neglecting nuclear recoil effects) then follows from Fermi's Golden Rule [37]:

$$\begin{aligned} \Gamma &= \int \frac{d^3k}{(2\pi)^3 2E_k} (2\pi) \delta(M_i - M_f - E_k) \frac{1}{2J_i + 1} \sum_{M_i, M_f, a} |\mathcal{M}|^2 \\ &= \left(\frac{k}{2\pi} \right) \frac{1}{2J_i + 1} \sum_{M_i, M_f, a} |\mathcal{M}|^2, \end{aligned} \quad (14)$$

where $k = \sqrt{(M_f - M_i)^2 - m_X^2}$. To evaluate this expression, the coupling current $\mathcal{J}^\mu(\vec{x})$ must be specified.

2.2 Currents and Matrix Elements for an Axial Vector

The hadronic current of Eq. (1) to be used in the nuclear matrix elements can be derived from quark- (and gluon-) level interactions using the same methods as in dark matter direct detection studies [38, 39, 40, 41]. In general, the fundamental quark-level interaction is matched onto an effective nucleon-level coupling based on chiral interactions. Since the typical momenta relevant for nuclear decays are very small compared to the pion or nucleon masses, $k/m_N \sim 10^{-2}(k/10 \text{ MeV})$, the non-relativistic expansions used for dark matter

calculations apply to an excellent approximation. These momenta are also much smaller than the inverse nuclear radius R^{-1} , with $kR \simeq 0.12 (k/10 \text{ MeV})(A/8)^{1/3}$. Working to leading order in k/m_N and kR , the general expression of Eq. (13) can be simplified considerably.

For an axial vector, we assume a coupling to quarks of the form

$$-\mathcal{L} \supset X_\mu \sum_q g_q \bar{q} \gamma^\mu \gamma^5 q, \quad (15)$$

where the sum runs over quark flavors. When this operator is inserted between a pair of nucleon states, the leading term in an expansion in k/m_N is [38, 39, 42, 43]

$$\langle N | \sum_q g_q \bar{q} \gamma^\mu \gamma^5 q | N \rangle = \delta_i^\mu \sigma^i \sum_q g_q \Delta q^{(N)}. \quad (16)$$

The coefficients $\Delta q^{(N)}$ have been extrapolated from data [44, 45, 46] and computed using lattice methods [47, 48, 49, 50, 51]. We use the recent combination of results in Ref. [52]:

$$\begin{aligned} \Delta u^{(p)} &= \Delta d^{(n)} = 0.897(27) \\ \Delta d^{(p)} &= \Delta u^{(n)} = -0.367(27) \\ \Delta s^{(p)} &= \Delta s^{(n)} = -0.026(4), \end{aligned} \quad (17)$$

where the proton-neutron equalities are expected to hold to within the listed uncertainties. The leading nucleon operator is often written in the isospin-inspired notation [38]

$$-\mathcal{L}_{eff} \supset \bar{N} (\vec{\sigma} \cdot \vec{X}) \frac{1}{2} (a_0 + a_1 \tau_3) N, \quad (18)$$

where τ_3 is the Pauli matrix in isospin space and

$$a_0 = (\Delta u^{(p)} + \Delta d^{(p)})(g_u + g_d) + 2g_s \Delta s^{(p)} \quad (19)$$

$$a_1 = (\Delta u^{(p)} - \Delta d^{(p)})(g_u - g_d). \quad (20)$$

The corresponding forms for the proton and neutron are $a_p = (a_0 + a_1)/2$ and $a_n = (a_0 - a_1)/2$. From this, we can identify the leading-order current operator to be used in nuclear matrix elements as [37]

$$\vec{\mathcal{J}}(\vec{x}) = \sum_{j=1}^A a_j \vec{\sigma}^j \delta(\vec{x} - \vec{x}_j), \quad \mathcal{J}^0(\vec{x}) \rightarrow 0, \quad (21)$$

where the sum runs over all nucleons. The corresponding expression for a (non-axial) vector can be found in Ref. [37].

Turning next to nuclear matrix elements, the current operator derived here can be applied to derive the transition operator in a spherical vector basis according to Eqs. (7–10). The longitudinal polarization of the massive vector gives non-zero \mathcal{L}_{J0} terms, while the transverse polarizations lead to $\mathcal{T}_{J,\mp\lambda}^{mag,el}$ contributions. However, to leading order in $(kR) \sim 0.1$ this full

machinery can be bypassed and the transition operator for an axial vector to be used in Eq. (2) simplifies to

$$\begin{aligned}
\mathcal{O} &= \int d^3x \sum_{\lambda} e^{-i\vec{k}\cdot\vec{x}} \epsilon_{\lambda}^* (\hat{e}_{\lambda}^* \cdot \vec{\mathcal{J}}) \\
&= \sum_{\lambda} \sum_{j=1}^A a_j \epsilon_{\lambda}^* (\hat{e}_{\lambda}^* \cdot \vec{\sigma}^j) + \mathcal{O}(kR) \\
&= \sum_{\lambda} \sum_{j=1}^A a_j \epsilon_{\lambda}^* (-1)^{\lambda} \sigma_{1,-\lambda}^j + \mathcal{O}(kR),
\end{aligned} \tag{22}$$

where in the last line we have expressed $\vec{\sigma}$ as a spherical tensor operator.

2.3 Application to the Atomki Anomaly in ${}^8\text{Be}$

As an application of the above formalism, we turn next to ${}^8\text{Be}$ transitions related to the anomaly seen at the MTA-Atomki facility [22]. The relevant ${}^8\text{Be}$ states, together with their properties, are listed in Table 1. Recall that an excess bump-like feature is seen in the isoscalar ${}^8\text{Be}^*(1^+) \rightarrow {}^8\text{Be}(0^+) + e^+e^-$ mode, but not in the related isovector ${}^8\text{Be}^{*'}(1^+) \rightarrow {}^8\text{Be}(0^+)$ transition. To evaluate whether the anomaly can be explained by a light axial vector with ${}^8\text{Be}^*(1^+) \rightarrow {}^8\text{Be}(0^+) + X$, the isoscalar and isovector decay rates to the axial vector are needed.

The initial and final nuclear states in the ${}^8\text{Be}^* \rightarrow {}^8\text{Be} + X$ and ${}^8\text{Be}^{*'} \rightarrow {}^8\text{Be} + X$ transitions have total angular momenta $J_i = 1$ and $J_f = 0$, so the transition operator must be a spherical tensor with $J = 1$. This implies

$$\langle J_f, M_f | \sigma_{1,-\lambda}^j | J_i, M_i \rangle \propto \delta_{M_i, \lambda}. \tag{23}$$

Using this feature, we can use Eq. (22) with the polarization expressions of Eq. (5) in Eq. (14) to write the total decay width as

$$\Gamma = \frac{k}{6\pi} \left[2 \left| \langle 0, 0 | \sum_{j=1}^A a_j \sigma_{1,-}^j | 1, 1 \rangle \right|^2 + \left(\frac{E_k}{m_X} \right)^2 \left| \langle 0, 0 | \sum_{j=1}^A a_j \sigma_{1,0}^j | 1, 0 \rangle \right|^2 \right]. \tag{24}$$

The sums in this expression can be split into neutron and proton pieces:

$$\sum_{j=1}^A a_j \sigma_{1,\lambda}^j = a_n \sum_{j=1}^{A-Z} \sigma_{1,\lambda}^{j,n} + a_p \sum_{j=1}^Z \sigma_{1,\lambda}^{j,p} \equiv a_n \hat{\sigma}_{1,\lambda}^n + a_p \hat{\sigma}_{1,\lambda}^p \tag{25}$$

where the hatted operators signify the spin operators acting on all nucleons of a given type in the nucleus. Using the Wigner-Eckart theorem, the various matrix elements can be written in terms of Wigner $3j$ symbols and reduced matrix elements. This yields

$$\langle 00 | \hat{\sigma}_{1,-1}^{p,n} | 11 \rangle = -\langle 00 | \hat{\sigma}_{1,0}^{p,n} | 10 \rangle = \frac{1}{\sqrt{3}} \langle 0 | | \sigma^{p,n} | | 1 \rangle. \tag{26}$$

Inserting these expressions into Eq. (24) above, we have

$$\Gamma = \frac{k}{18\pi} \left(2 + \frac{E_k^2}{m_X^2} \right) |a_n \langle 0 | \sigma^n | 1 \rangle + a_p \langle 0 | \sigma^p | 1 \rangle|^2. \quad (27)$$

Thus, the required nuclear input to the decay width consists of two reduced matrix elements (for each of the two relevant ^8Be excited states).

The corresponding matrix element for electromagnetic transitions must also have $J = 1$. Taking parity into account, it corresponds to operators of the form $\mathcal{T}_{J=1,\pm\lambda}^{mag}$ in Eq. (6). For obvious reasons, these transitions are referred to as $M1$ [36, 37].

3 *Ab Initio* Calculation of ^8Be Matrix Elements

To evaluate the nuclear matrix elements, we perform *ab initio* calculations using realistic nuclear forces. In the present case, this means that we solve the full quantum mechanical system of eight nucleons (for ^8Be) interacting with each other through forces derived from chiral effective field theory using the in-medium similarity renormalization group (IM-SRG) [53, 54, 55], a recently-developed many-body method.

3.1 Chiral Interactions

The inter-nucleon interactions used in our calculation are derived from chiral effective field theory and include two- and three-nucleon components. For the two-nucleon (NN) interaction, we use the result of Entem and Machleidt, Ref. [56], derived at next-to-next-to-next-to-leading order (N³LO) in the chiral expansion, with a non-local regulator with cutoff $\Lambda_{NN} = 500$ MeV. Importantly, this interaction includes the Coulomb force as well as nuclear isospin symmetry-breaking terms [56]. For the three-nucleon (3N) interaction, we use the local N²LO interaction of Navrátil, Ref. [57], with cutoff $\Lambda_{3N} = 400$ MeV¹ and the two low energy constants c_D and c_E fit to the triton half-life and $A = 3$ binding energies [58].

To facilitate the convergence of the many-body calculation, the NN and 3N interactions are softened by the similarity renormalization group (SRG) to a momentum scale $\lambda_{\text{SRG}} = 2.0$ fm⁻¹ [59, 60]. We designate this interaction SRG 2.0. As a check, we also employ the same interaction softened to a momentum scale $\lambda_{\text{SRG}} = 1.88$ fm⁻¹. Since the SRG is a unitary transformation (up to induced four-body forces), the end results should be approximately independent of our choice of λ_{SRG} . The lower cutoff Λ_{3N} mentioned above was used in Ref. [61], and in many subsequent works (see e.g. [62, 63, 64, 65, 66], because – in the region around ^{16}O – it produced results with a much weaker dependence on λ_{SRG} , indicating smaller induced 4N effects. We also compare with calculations using the same N³LO NN

¹While the regulators used in the NN and 3N sectors are not the same, there is no consensus as to how to consistently regulate the NN and 3N forces. Fortunately, the present results are not sensitive to these details.

force but with the non-local N²LO 3N interaction of Ref. [67], which is not consistently SRG-evolved, but instead has the 3N contact terms fit to reproduce the ³H binding energy and the ⁴He radius. The NN force is SRG softened to $\lambda_{SRG} = 1.8 \text{ fm}^{-1}$, while the 3N force uses a regulator $\Lambda_{3N} = 2.0 \text{ fm}^{-1} \approx 395 \text{ MeV}$. This interaction – which was previously used to study nuclear matter [67, 68], *sd*-shell nuclei [69], and selected calcium [70, 71] and nickel [72] isotopes – is designated EM 1.8/2.0.

3.2 Many-Body Calculation

We perform the many-body calculation using the IM-SRG, which we summarize below. A more detailed review may be found in Ref. [54]. In this method, the Hamiltonian

$$H = T_{\text{rel}} + V_{\text{NN}} + V_{\text{3N}} , \quad (28)$$

consisting of the relative kinetic energy plus the NN and 3N inter-nucleon interactions, is evaluated in a harmonic oscillator basis with frequency $\hbar\omega$. Since the harmonic oscillator eigenstates form a complete basis, an arbitrary wave function may be represented using an infinite number of basis states, independent of the choice of $\hbar\omega$. In our calculation, we apply a single-particle truncation $2n + \ell \leq e_{\text{max}}$, where n is the radial quantum number and ℓ is the orbital angular momentum, so that our results would become exact in the limit $e_{\text{max}} \rightarrow \infty$.

Before implementing the IM-SRG, we begin by performing a spherical Hartree-Fock calculation of the ⁸Be ground state explicitly including the 3N interaction. The interaction is then normal-ordered with respect to the Hartree-Fock ground state,² and the residual 3N force is discarded. Note that while we discard the residual 3N piece, we retain most of the original 3N force through its normal-ordered 0-, 1-, and 2-body parts. This approximation has been shown to be sufficient to capture the effects of 3N forces in the *p*-shell, such as the 1⁺-3⁺ spin ordering in ¹⁰B [73, 74].

Next, the IM-SRG is used to perform a unitary transformation U which decouples a small valence space from the larger Hilbert space, producing an effective valence space interaction which approximately reproduces a subset of the eigenstates of the full space [75, 66]. In the case of ⁸Be, we decouple the *0p* shell model space. To achieve this, we write the transformed Hamiltonian as [76]

$$\begin{aligned} \tilde{H} &= U H U^\dagger \\ &= e^\Omega H e^{-\Omega} \\ &= H + [\Omega, H] + \frac{1}{2!} [\Omega, [\Omega, H]] + \frac{1}{3!} [\Omega, [\Omega, [\Omega, H]]] + \dots \end{aligned} \quad (29)$$

where the operator $\Omega = -\Omega^\dagger$ is the generator of the transformation, and the square brackets indicate a commutator. While the last line in Eq. (29) contains an infinite number of terms,

²As discussed in Ref [73], because we use a spherical formalism to treat an open-shell system, the reference is not a wave function but instead a particle-number violating ensemble, or mixed-state, reference. However the states produced in the final calculation are proper wave functions with good particle number.

arbitrarily high precision may be obtained with a finite number of terms for well-behaved transformations U . The task is then to obtain an operator Ω that produces a decoupled Hamiltonian. We achieve this by parameterizing Ω in terms of a flow parameter s and an operator $\eta(s)$ that determines the direction of the flow, and integrating a flow equation

$$\begin{aligned}
e^{\Omega(s+ds)} &= e^{\eta(s)ds} e^{\Omega(s)} \\
&\Downarrow \\
\Omega(s+ds) &= \Omega(s) + \eta(s)ds + \frac{1}{2}[\eta(s), \Omega(s)] + \dots,
\end{aligned}
\tag{30}$$

making use of the Baker-Campbell-Hausdorff formula. We choose [77]

$$\eta(s) \equiv \frac{1}{2} \tan^{-1} \left(\frac{2\tilde{H}_{od}(s)}{\Delta(s)} \right) - h.c.
\tag{31}$$

where $\Delta(s)$ is an energy denominator given by the difference of the expectation values of $H(s)$ for the bra and ket states, and the so-called off-diagonal part of the Hamiltonian, \tilde{H}_{od} , is the part we wish to suppress. In the present case it is given by those terms which connect valence space configurations to configurations outside the valence space. The arctangent in Eq. (31) is motivated by the solution of a two-level system, and ensures that no over-rotation is performed, even in the case of small denominators. In Eqs. (29,30), we retain only up to normal-ordered two-body operators. This approximation, denoted IM-SRG(2), is the main approximation of the method and typically produces absolute binding energies within approximately 1% of the full solution. Evidently, as the Hamiltonian is decoupled, \tilde{H}_{od} is suppressed, $\eta(s) \rightarrow 0$, and $\Omega(s)$ approaches a fixed point.

At this point, the valence space forms a sub-block that is fully decoupled from the full Hilbert space. We diagonalize \tilde{H} in the valence space, using the shell model code NuShellX [78] to obtain the final wave functions. All transition operators \mathcal{O} are consistently transformed using Eq. (29) replacing $H \rightarrow \mathcal{O}$, as presented in Ref. [79], and are then evaluated with the shell model wave functions.

3.3 Results for ${}^8\text{Be}$

In Fig. 1 we show the resulting excitation spectra in ${}^8\text{Be}$ up to 20 MeV for a few selected combinations of interactions and model spaces, as well as the experimentally measured spectrum. We find a reasonable reproduction of the spectrum for all cases, noting that broad resonances such as the low-lying 2^+ and 4^+ states are typically poorly represented in a harmonic oscillator basis. Fortunately, the states of interest are the lowest two 1^+ states, corresponding to ${}^8\text{Be}^*$ and ${}^8\text{Be}^{*f}$ in Table 1, which are narrow and reproduced well by the calculations.

The specific quantities of interest for the present work are the transition matrix elements relevant to Eq. (27) involving the ${}^8\text{Be}^*$ and ${}^8\text{Be}^{*f}$ states. An important factor in the description of these states, and particularly for the transition rates, is their isospin content. For example, owing essentially to the opposite signs of the proton and neutron spin g factors,

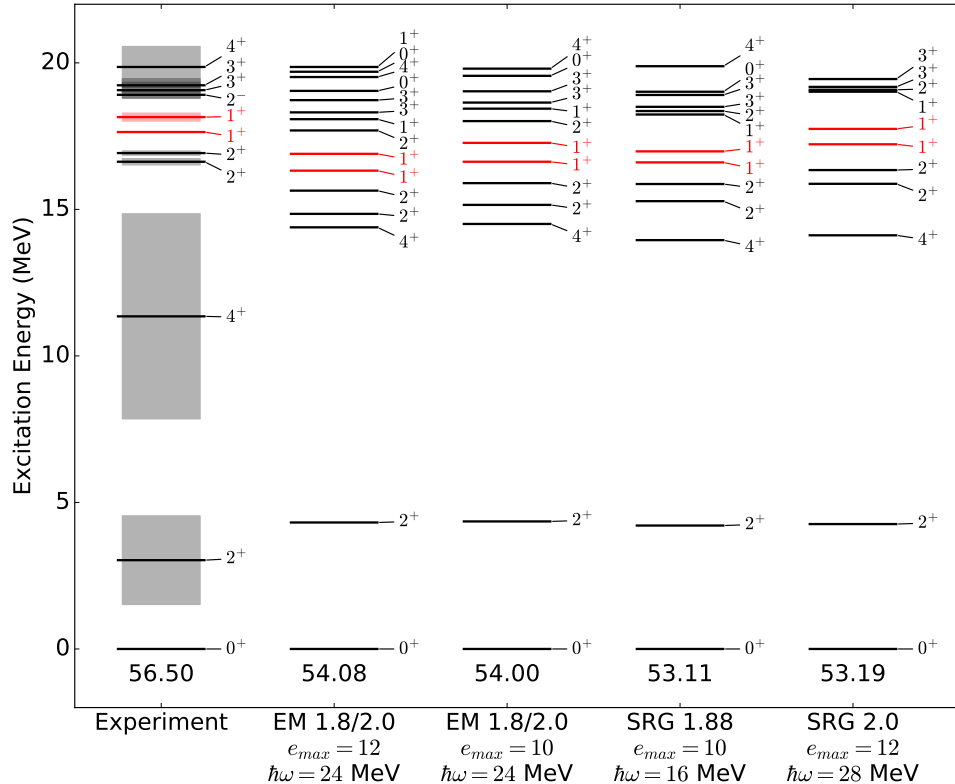


Figure 1: Experimental spectrum of ${}^8\text{Be}$ labeled with total angular momentum and parity, compared with calculated spectra using the following interactions and model space parameters (see text for details). The shaded gray bands on the experimental spectrum indicate the width of the state. The 1^+ states of interest are highlighted in red. Binding energies in MeV are also given beneath the ground states.

isovector $M1$ (magnetic dipole) transitions dominate over isoscalar $M1$ transitions in $N = Z$ nuclei (see, e.g., Ref. [80]), while the opposite is true for an axial vector coupling. This feature can be seen in the $M1$ photon transition rates Γ_γ of the ${}^8\text{Be}^*$ and ${}^8\text{Be}^{*'}$ states listed in Table 1, which are much larger for the ${}^8\text{Be}^{*'}$ ($T \simeq 1$) state than the ${}^8\text{Be}^*$ ($T \simeq 0$) state. Note, however, that these isospin assignments are only approximate and each physical state is a mixture of isospin eigenstates.

Isospin mixing in this context is delicately sensitive to the energy splitting between the two 1^+ states, and to the isospin breaking terms in the interaction. As a result, it is difficult to calculate this isospin mixing fraction with high precision. However, since both the vector ($M1$) and axial vector transition rates depend on the mixing, the two quantities become correlated. We adopt the strategy used in Refs. [70, 81, 72] to predict the axial vector matrix elements using their correlation with the isospin mixing and the known $M1$ transition strengths.³

³The isospin mixing fraction is not an observable quantity, but it is a useful heuristic to understand

Let us denote the predominantly isoscalar ${}^8\text{Be}^*$ and isovector ${}^8\text{Be}'$ states by $|\mathcal{S}\rangle$ and $|\mathcal{V}\rangle$, respectively, and the pure isospin eigenstates by $|T=0\rangle$ and $|T=1\rangle$. Since our calculation methods violate isospin from the beginning, we do not have direct access to the pure isospin states. Instead, we follow Ref. [82] and treat the isospin mixing as two-level mixing, so that the physical states are given by

$$\begin{aligned} |\mathcal{S}\rangle &= \beta|T=0\rangle + \alpha|T=1\rangle \\ |\mathcal{V}\rangle &= -\alpha|T=0\rangle + \beta|T=1\rangle . \end{aligned} \quad (32)$$

The isospin mixing parameters may be obtained by

$$|\alpha|^2 = \frac{1}{2}\langle\mathcal{S}|\hat{T}^2|\mathcal{S}\rangle \quad , \quad |\beta|^2 = \frac{1}{2}\langle\mathcal{V}|\hat{T}^2|\mathcal{V}\rangle \quad , \quad \alpha\beta = \frac{1}{2}\langle\mathcal{S}|\hat{T}^2|\mathcal{V}\rangle \quad (33)$$

where \hat{T}^2 is the squared isospin operator.

Meson exchange currents (MEC) in the nuclear current operators have not been included in our calculation. The effect of MECs on $M1$ transitions in ${}^8\text{Be}$ was investigated in Ref. [82] using a quantum Monte Carlo approach, yielding a 28% correction to the isovector $M1$ matrix element. To account for this, we correct the $M1$ matrix elements obtained in our calculation by

$$\delta_{MEC}(\mathcal{S}) = 0.28 (\alpha^2\langle\mathcal{S}||M1||\mathcal{S}\rangle + \alpha\beta\langle\mathcal{V}||M1||\mathcal{V}\rangle) \quad (34)$$

$$\delta_{MEC}(\mathcal{V}) = 0.28 (\beta^2\langle\mathcal{V}||M1||\mathcal{V}\rangle + \alpha\beta\langle\mathcal{S}||M1||\mathcal{S}\rangle) . \quad (35)$$

The leading MEC correction to the axial current at low momentum is a two-body operator. We follow Ref. [83] and treat the two-body contribution of this two-body operator by normal-ordering with respect to a Fermi gas. This leads to a fractional correction to the isovector part of the current of

$$\delta a_1 = -\frac{\rho}{F_\pi^2} I(\rho, P=0) \left[\frac{1}{3}(2c_4 - c_3) + \frac{1}{6m_N} \right] , \quad (36)$$

where ρ is the nucleon density, F_π is the pion decay constant, c_3 and c_4 are low energy constants of the NN interaction, m_N is the nucleon mass, and the quantity $I(\rho, P=0)$, defined as

$$I(\rho, P=0) = 1 - \frac{3m_\pi^2}{k_F^2} + \frac{m_\pi^3}{2k_F^3} \cot^{-1} \left(\frac{m_\pi^2 - k_F^2}{2m_\pi k_F} \right) , \quad (37)$$

is due to summation in the exchange term. In Eq. (37), $k_F = (3\pi^2\rho/2)^{1/3}$ is the Fermi momentum of the Fermi gas, and m_π is the pion mass. Taking $\rho \approx 0.10 \text{ fm}^{-3}$ yields $\delta a_1 \approx -0.25$. We incorporate this fractional correction by scaling the proton axial vector matrix elements by $(1 + \frac{1}{2}\delta a_1)$ and the neutron matrix elements by $(1 - \frac{1}{2}\delta a_1)$.

In Fig. 2 we show the matrix elements of the $M1$ transition operator (corrected for MECs) and the proton and neutron spin operators σ_p and σ_n connecting the ground state to each of the lowest two 1^+ states, calculated with the chiral interactions described above. For each

the correlation between the $M1$ and axial vector matrix elements. Using this correlation directly produces similar results.

Matrix element	Prediction
$\langle 0^+ M1 \mathcal{V} \rangle$	0.76(12) μ_N
$\langle 0^+ \sigma_p \mathcal{V} \rangle$	0.102(28)
$\langle 0^+ \sigma_n \mathcal{V} \rangle$	-0.073(29)
$\langle 0^+ \sigma_p \mathcal{S} \rangle$	-0.047(29)
$\langle 0^+ \sigma_n \mathcal{S} \rangle$	-0.132(33)

Table 2: Predicted nuclear matrix elements for the various transitions of interest, obtained by the correlation method described in the text. The predicted value of the $M1$ matrix element for the physical isovector-like state (\mathcal{V}) is consistent with the experimental value $0.84(7) \mu_N$.

interaction, points are shown for a range of basis truncations e_{max} and oscillator frequencies $\hbar\omega$, establishing a clear correlation between the matrix elements and the isospin mixing. In the figures we multiply the σ matrix elements by the sign of the $M1$ matrix element to eliminate effects due to the (arbitrary) relative sign of the initial and final wave functions.

As the $|\mathcal{S}\rangle$ state is predominantly $T = 0$, MEC corrections to the decay of this state are smaller and we expect this calculation to be more accurate than for the decay of the $|\mathcal{V}\rangle$ state. In the upper left panel of Fig. 2 we observe a strong correlation between the $\langle 0^+ | M1 | \mathcal{S} \rangle$ matrix element and the isospin mixing, indicated by the purple band. We use this correlation and the experimentally known $M1$ strength to constrain the isospin mixing in our calculations, and find $|\alpha| = 0.35(8)$. This is larger than the value $\alpha = 0.21(3)$ extracted in Ref. [84] from a fit to data based on shell model calculations and a bare $M1$ operator, but consistent with $\alpha = 0.31(4)$ obtained in Ref. [82] that does include MEC corrections. With this constraint, we make predictions for the other matrix elements, indicated by the hashed boxes in Fig. 2. Our results are summarized in Table 2.

4 The ${}^8\text{Be}$ Anomaly from an Axial Vector

Equipped with the nuclear transition matrix elements and the formalism described above, we can now address the Atomki ${}^8\text{Be}$ anomaly [22] in terms of a light axial vector. Recall that the anomaly is seen in isoscalar ${}^8\text{Be}^* \rightarrow {}^8\text{Be}$ transitions, but not in isovector ${}^8\text{Be}^{*'} \rightarrow {}^8\text{Be}$. We find that this feature can arise naturally for decays to a light axial vector.

4.1 Isoscalar ${}^8\text{Be}^* \rightarrow {}^8\text{Be} + X$ Transitions

The original experimental paper reporting the ${}^8\text{Be}$ anomaly also provided an interpretation in terms of a light vector boson [22]. The best fit mass and decay rate explaining the observed deviation from the predicted internal pair creation signal assuming $\text{BR}(X \rightarrow e^+e^-) = 1$ were

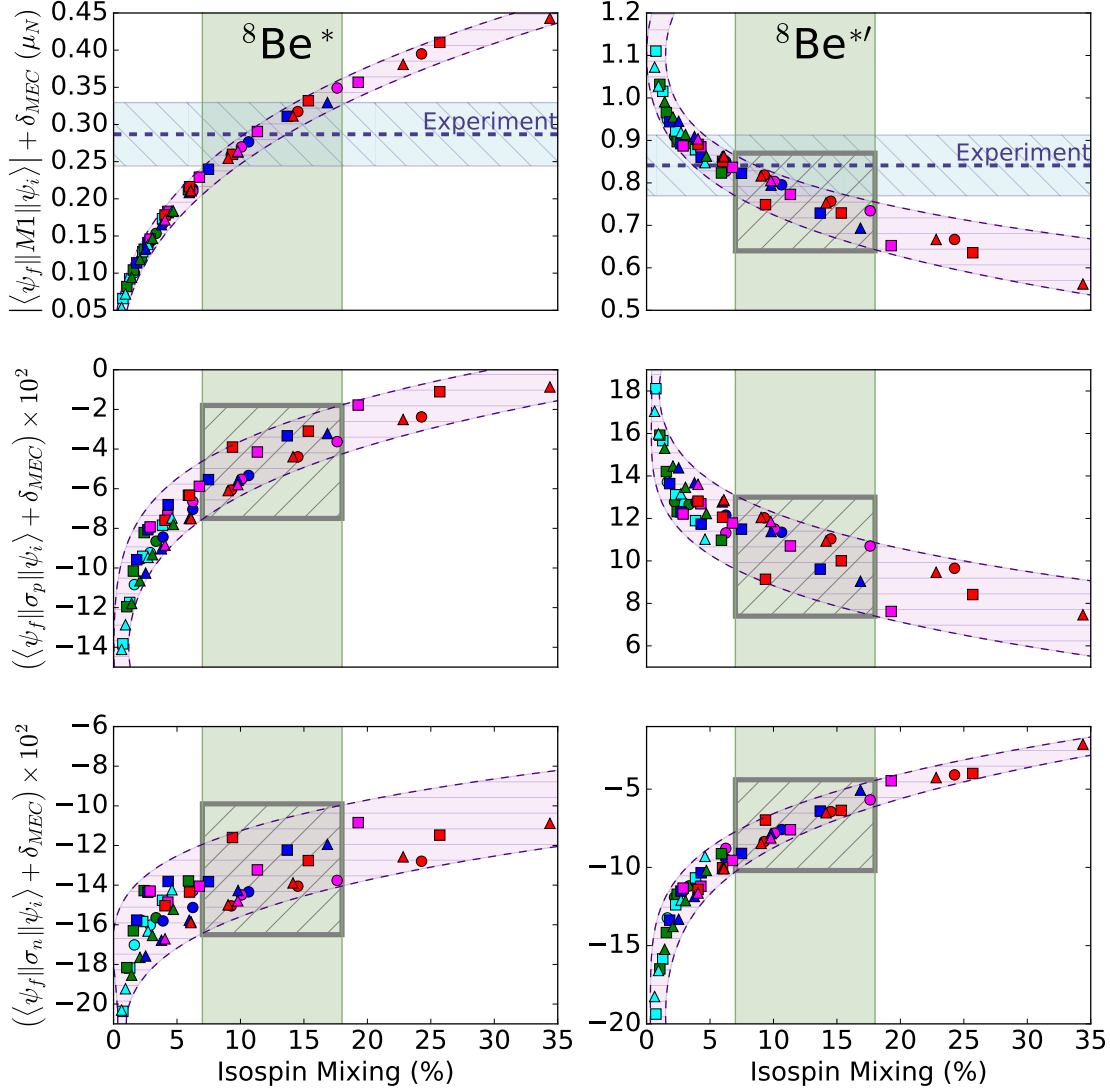


Figure 2: Reduced transition matrix elements for the $M1$, σ_p , and σ_n operators between the $|\mathcal{S}\rangle$ ($^8\text{Be}^*$, left column) and the $|\mathcal{V}\rangle$ ($^8\text{Be}^{*!}$, right column) 1^+ excited states and the ground state of ^8Be as a function of the isospin mixing fraction $|\alpha|^2$. Approximate corrections for meson exchange currents have been included. Circles indicate results using the SRG 1.88 interaction, triangles indicate the SRG 2.0 interaction, and squares indicate the EM 1.8/2.0 interaction. The single-particle basis truncations are indicated by different colors: $e_{max} = 4$ (cyan), 6 (green), 8 (blue), 10 (magenta), 12 (red). We include points for oscillator frequencies $\hbar\omega=12, 16, 20, 24,$ and 28 MeV. The $M1$ matrix element for the $T \simeq 0, J^P = 1^+$ state in the upper left is used to constrain the range of the isospin mixing fraction, which is then used to make predictions for the other matrix elements, indicated by the hashed boxes.

reported to be

$$m_X \simeq 16.7 \text{ MeV}, \quad \frac{\Gamma_{^8\text{Be}^* \rightarrow ^8\text{Be} X}}{\Gamma_{^8\text{Be}^* \rightarrow ^8\text{Be} \gamma}} \simeq 5.8 \times 10^{-6}, \quad (38)$$

with $\Gamma_{^8\text{Be}^* \rightarrow ^8\text{Be}\gamma} \simeq (1.9 \pm 0.4) \text{ eV}$ [23]. Best-fit points for fixed higher masses were subsequently presented in Ref. [25], citing a private communication with the authors of Ref. [22]. These are:

$$\begin{aligned} m_X \simeq 17.3 \text{ MeV}, & \quad \frac{\Gamma_{^8\text{Be}^* \rightarrow ^8\text{Be}X}}{\Gamma_{^8\text{Be}^* \rightarrow ^8\text{Be}\gamma}} \simeq 2.3 \times 10^{-6} \\ m_X \simeq 17.6 \text{ MeV}, & \quad \frac{\Gamma_{^8\text{Be}^* \rightarrow ^8\text{Be}X}}{\Gamma_{^8\text{Be}^* \rightarrow ^8\text{Be}\gamma}} \simeq 5.0 \times 10^{-7}. \end{aligned} \tag{39}$$

It is likely that the overall fit to the data is worse for these higher masses [22]. The best-fit mass and width for an axial vector may also differ due to the potentially slightly different angular distribution of e^+e^- pairs relative to a purely vector coupling. However, in both cases more information about the experimental apparatus and analysis would be needed to investigate these features in detail.

Starting with the masses and decay widths listed above, we compute the range of quark couplings to the axial vector that explain the ^8Be anomaly. To do so, we use Eqs. (19,20) to relate the quark couplings g_q to the coefficients a_p and a_n , and then evaluate the decay width of Eq. (27) varying the nuclear matrix elements listed in Table 2, as well as the nucleon coefficients in Eq. (17), across their uncertainty bands. The final results are shown in Fig. 3 assuming $g_u < 0$, $g_d > 0$, $g_s = g_d$, and $\text{BR}(X \rightarrow e^+e^-) = 1$.

The ranges of potential axial vector quark couplings for the ^8Be anomaly are fairly large due to the significant uncertainties on the values of the nuclear matrix elements. If the anomaly is confirmed in future experiments, it will be important to increase the precision of the nuclear calculation. Despite these uncertainties, we can draw some preliminary conclusions about the parameter space consistent with the anomaly. In general, we find that $\text{Max}(|g_u|, |g_d|) \gtrsim 10^{-5}$ is required to explain the result. Note that this is significantly smaller than the quark couplings needed for the protophobic vector explanation of the anomaly studied in Refs. [24, 25]. This can be understood in terms of the leading partial wave for the decay, with the axial vector decay proceeding at $\ell = 0$ and proportional to $k/m_X \ll 1$ (from phase space), while the vector decay proceeds at $\ell = 1$ with a rate proportional to k^3/m_X^3 [24].

4.2 Isovector $^8\text{Be}^{*'} \rightarrow ^8\text{Be} + X$ Transitions

The transition rate for $^8\text{Be}^{*'} \rightarrow ^8\text{Be} + X$ can be computed in the same way as discussed above. Since no significant excess was seen in $^8\text{Be}^{*'} \rightarrow ^8\text{Be} + e^+e^-$ [22, 85], we must check whether the quark couplings g_q that explain the anomaly in the isoscalar channel are consistent with the data in the isovector mode.

The condition we impose on the isovector channel for a given vector boson mass follows that used in Ref. [24]:

$$\frac{\Gamma_{^8\text{Be}^* \rightarrow ^8\text{Be}X}}{\Gamma_{^8\text{Be}^* \rightarrow ^8\text{Be}\gamma}} > 5 \times \frac{\Gamma_{^8\text{Be}^{*'} \rightarrow ^8\text{Be}X}}{\Gamma_{^8\text{Be}^{*'} \rightarrow ^8\text{Be}\gamma}}. \tag{40}$$

This (approximate) requirement is obtained by assuming that the statistical uncertainties

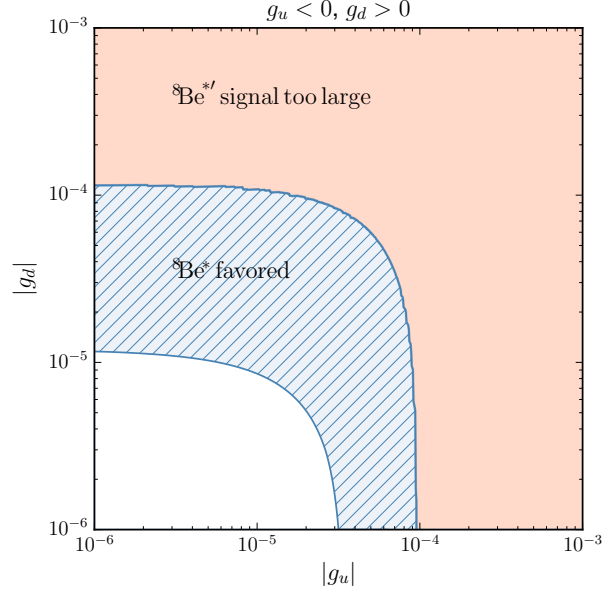


Figure 3: Quark couplings required to explain the MTA-Atomki ${}^8\text{Be}$ anomaly via a light axial vector assuming $g_u < 0$, $g_d > 0$, and electron couplings such that $\text{BR}(X \rightarrow e^+e^-) = 1$ is prompt. The hatched band was obtained by considering $m_X = 16.7, 17.3, 17.6$ MeV, imposing the corresponding requirements in Eqs. (38)-(39) to explain the MTA-Atomki result, then varying the relevant nuclear matrix elements and nucleon coefficients $\Delta u^{(p),(n)}$, $\Delta d^{(p),(n)}$, $\Delta s^{(p),(n)}$ across their allowed ranges. Points below the hatched region feature couplings too small to explain the observed ${}^8\text{Be}^*$ transition rate for the three masses considered. The orange region to the upper right is excluded by the non-observation of an excess in the isovector ${}^8\text{Be}^{*'} \rightarrow {}^8\text{Be} + e^+e^-$ channel for $m_X = 16.7$ - 17.6 MeV.

on the ${}^8\text{Be}^{*'}$ transition are comparable to those for the ${}^8\text{Be}^*$ transition, and that the ratios of the pair creation to electromagnetic transition rates are similar for both states.⁴ A more precise upper bound on the isovector transition rate would require additional information about the MTA-Atomki detector sensitivities.

In Fig. 3 we show the impact of the ${}^8\text{Be}^{*'}$ condition of Eq. (40) on the possible ranges g_u and g_d . Values of the couplings for which Eq. (40) is not satisfied for any value of the nuclear matrix elements within the ranges quoted in Table 2, nucleon coefficients within the ranges of Eq. (17), and $m_X \in [16.7, 17.6]$ MeV are indicated by the orange shaded region in the figure. The limit is the strongest model-independent constraint on the parameter space shown, highlighting the potential for nuclear decay experiments to probe previously unexplored theories of light vector bosons. The hatched region in Fig. 3 comprises the couplings that can be consistent with both the ${}^8\text{Be}^*$ anomaly and the ${}^8\text{Be}^{*'}$ constraint. Roughly, this requires $\text{Max}(|g_u|, |g_d|) \lesssim 10^{-4}$.

The results of Fig. 3 also reflect that the ${}^8\text{Be}^{*'} \rightarrow {}^8\text{Be} + X$ transition rate can be suppressed

⁴We thank Jonathan Feng for clarification on this point.

relative to that of the ${}^8\text{Be}^* \rightarrow {}^8\text{Be} + X$ mode for an axial vector, which is an important virtue of the axial vector interpretation. This effect is dynamical, as can be seen by comparing the relative sizes and signs of the reduced matrix elements in Table 2. In particular, the axial vector matrix elements are of similar size for both the isoscalar and isovector states, while the $M1$ matrix element relevant to the denominators in Eq. (40) is much larger for the isovector than the isoscalar. This leads to a suppression of the isovector ratio in Eq. (40) relative to the isoscalar that is not possible for a light gauge boson with only vector couplings, for which the relevant matrix elements are also proportional to those for the $M1$ transition. One must then rely on kinematic suppression of the vector contribution to this transition by pushing the mass of the new particle closer to the ${}^8\text{Be}^{*'}$ threshold [24, 25], which appears to worsen the fit to experimental data.

5 Constraints on Axial Vectors for the ${}^8\text{Be}$ Anomaly

In addition to the requirements on the quark couplings discussed above, the axial vector must couple to leptons to allow it to decay to e^+e^- pairs within the Atomki detector. Lepton couplings also typically arise when the axial vector is embedded in a consistent UV-complete theory. Together, these quark and lepton couplings imply significant constraints on light vector explanations of the ${}^8\text{Be}$ anomaly. In this section we investigate the most significant constraints on a light vector with axial quark couplings, making extensive use of the recent related analyses of Refs. [9, 25, 33]. These bounds will be applied to a UV complete theory of a light axial vector in the section to follow.

To focus our study on the most important constraints on light axial vector explanations of the ${}^8\text{Be}$ anomaly, we adopt the following assumptions:

1. The light vector X has only axial couplings to quarks, and these couplings are generation independent to avoid flavor mixing.
2. Both vector and axial couplings to charged leptons are allowed for the light vector:

$$\mathcal{L} \supset X_\mu \sum_i \bar{\ell}_i (g_i^V \gamma^\mu + g_i^A \gamma^\mu \gamma^5) \ell_i, \quad (41)$$

where the sums run over the charged leptons of the Standard Model. These couplings are again assumed to be generation independent.

3. The couplings of the vector boson to neutrinos vanish. This circumvents stringent constraints from electron-neutrino scattering experiments [33, 86, 87, 88], and guarantees $\text{BR}(X \rightarrow e^+e^-) = 1$ in the absence of other light states.

With these assumptions, we compute the most significant constraints on light vectors due their lepton and quark couplings.

5.1 Lepton Coupling Constraints

For a light vector X to explain the ^8Be anomaly, its couplings to electrons must be large enough that it decays inside the Atomki detector. As pointed out in Refs. [25], this implies

$$\frac{\sqrt{(g_e^V)^2 + (g_e^A)^2}}{e} \gtrsim 1.3 \times 10^{-5}. \quad (42)$$

Beyond this basic requirement, the lepton couplings of a light vector are constrained by lepton anomalous magnetic moments, beam dump searches, electron-positron collider experiments, and tests of parity violation in Møller scattering.

5.1.1 Anomalous Magnetic Moments

The anomalous magnetic moments of the charged leptons are affected by a light vector that couples to them. The corresponding shifts in $a_{e,\mu} \equiv (g - 2)_{e,\mu}$ for a general vector boson X with both vector and axial couplings to leptons are [9]

$$\begin{aligned} \delta a_e &= \frac{(g_e^V)^2}{4\pi^2} \int_0^1 dx \frac{x^2(1-x)}{x^2 + \frac{m_x^2}{m_e^2}(1-x)} - \frac{(g_e^A)^2}{4\pi^2} \frac{m_e^2}{m_x^2} \int_0^1 dx \frac{2x^3 + (x-x^2)(4-x)\frac{m_x^2}{m_e^2}}{x^2 + \frac{m_x^2}{m_e^2}(1-x)} \\ \delta a_\mu &= \frac{(g_\mu^V)^2}{4\pi^2} \int_0^1 dx \frac{x^2(1-x)}{x^2 + \frac{m_x^2}{m_\mu^2}(1-x)} - \frac{(g_\mu^A)^2}{4\pi^2} \frac{m_\mu^2}{m_x^2} \int_0^1 dx \frac{2x^3 + (x-x^2)(4-x)\frac{m_x^2}{m_\mu^2}}{x^2 + \frac{m_x^2}{m_\mu^2}(1-x)}. \end{aligned} \quad (43)$$

In general, the axial coupling of a light vector to leptons leads to negative contributions to their anomalous magnetic moments. In the case of the muon, where the SM prediction is already lower than the measured value by about 3.4σ [89, 90], a light vector with purely axial couplings to muons worsens the disagreement.

The interpretation of the measurement of a_μ as a constraint requires some care, since a naive application of the experimental result would also exclude the Standard Model. The disagreement between measurement and the SM prediction is about $2.9 \pm 0.8 \times 10^{-9}$ [89, 90]. To obtain a constraint from a_μ , we demand that the contribution to δa_μ from the axial vector be less than the 2σ uncertainty (in either direction) of the discrepancy between experiment and the SM: $|\delta a_\mu| \lesssim 1.6 \times 10^{-9}$. For $m_X \simeq 17$ MeV, this amounts to

$$\left| -(g_\mu^A)^2 + 9 \times 10^{-3} (g_\mu^V)^2 \right| \lesssim 1.6 \times 10^{-9}. \quad (44)$$

Let us also emphasize that numerous proposals have been made to explain the disagreement in a_μ , and many of them invoke weak-scale physics that would not significantly alter the other low-energy observables considered here. In this context, our requirement on $|\delta a_\mu|$ from a light axial vector corresponds to an absence of a strong cancellation with other contributions.

For the a_e constraint, we impose $-26 \times 10^{-13} < \delta a_e \lesssim 8 \times 10^{-13}$ [91].

5.1.2 Electron Beam Dump Experiments

Light vector bosons can be produced at electron beam dump experiments [11]. For $m_X \simeq 17$ MeV, the most stringent constraint comes from the SLAC E141 experiment [92], which requires [16, 33]

$$\frac{\sqrt{(g_e^A)^2 + (g_e^V)^2}}{e} \gtrsim 2 \times 10^{-4}. \quad (45)$$

In this regime, the vector X would have decayed before reaching the detector. Other electron beam dump experiments yield less stringent bounds on the couplings; see Refs. [25, 33] for a more comprehensive discussion of these constraints.

5.1.3 Electron-Positron Colliders

A light axial vector coupling to electrons can be produced at e^+e^- experiments. The KLOE2 search for $e^+e^- \rightarrow X\gamma$, $X \rightarrow e^+e^-$ sets a limit of [25, 33]

$$\frac{\sqrt{(g_e^A)^2 + (g_e^V)^2}}{e} \lesssim 2 \times 10^{-3} \quad (46)$$

for $m_X \simeq 17$ MeV. The BABAR experiment also searched for $e^+e^- \rightarrow X\gamma$, $X \rightarrow \ell^+\ell^-$, but only down to $m_X \gtrsim 20$ MeV [93].

5.1.4 Parity Violating Møller Scattering

Mixed axial-vector couplings of X to leptons induces parity violation in Møller scattering. This was studied in the E158 experiment at SLAC [94], and for $m_X \simeq 17$ MeV produces the constraint [33]

$$|g_e^V g_e^A| \lesssim 1 \times 10^{-8}. \quad (47)$$

Aside from a_μ , this limit gives the the most stringent upper bound on lepton couplings in the UV-complete scenario we discuss below.

5.2 Quark Coupling Constraints

Light vector bosons can be constrained further if they couple to both quarks and leptons, as required to explain the ^8Be anomaly. The two most important quark coupling constraints on this scenario, and given our assumptions, come from η decays and proton beam dump experiments.

5.2.1 Rare η Decays

New light particles can contribute to rare decays of the η meson. As discussed in Refs. [33, 95], the decay amplitude for $\eta \rightarrow \mu^+\mu^-$ receives a new contribution from the axial vector

approximately proportional to $g_\mu^A(g_u + g_d - cg_s)$ that interferes with the SM contribution. Here c is a real $\mathcal{O}(1)$ number that depends on the precise values of the $\eta - \eta'$ mixing parameters used. This new contribution can produce a significant shift in the decay width for this mode relative to the SM alone, which agrees with data to within about 1σ . To determine the corresponding constraint, we evaluate the $\eta \rightarrow \mu^+\mu^-$ partial width following Ref. [95], and demand that the net shift be less than the 2σ uncertainty on the SM prediction. This corresponds roughly to

$$\frac{g_\mu^A(g_u + g_d - 1.5g_s)}{(m_X/\text{MeV})^2} \lesssim 4 \times 10^{-10}. \quad (48)$$

Note that this differs slightly from the bound quoted in Ref. [33] obtained using a different value for the $\eta - \eta'$ mixing angle; the impact of this difference is negligible on the parameter space of interest.

5.2.2 Proton Fixed Target Experiments

Proton fixed target experiments also constrain the quark couplings of the vector, this time in combination with the electron couplings. In particular, the limits from the ν -Cal I experiment at the IHEP U70 accelerator provide bounds on X production from bremsstrahlung off the proton beam [96]. In dark photon models, the corresponding bound is $\epsilon^2 \lesssim 3.7 \times 10^{-13}$ or $\epsilon^2 \gtrsim 2.5 \times 10^{-9}$; very small couplings are allowed because most of the dark photons decay before the detector, while larger couplings imply that the dark photons decay well after.

To recast this constraint onto the axial vector scenario, we reinterpret the constraint of the ν -Cal experiment on the number of dark vector bosons N_{sig} produced by bremsstrahlung off the initial beam that decay inside the fiducial volume of the detector. This number is given by

$$N_{\text{sig}} = N_{\text{tot}} \eta \int dE_X \frac{dN}{dE_X} P(E_X) \quad (49)$$

where N_{tot} is the total number of proton collision events, $P(E_X)$ is the probability for the vector to decay inside the detector, dN/dE_X is the differential X vector production rate per proton interaction, and η is the efficiency of the detector. The probability $P(E_X)$ is given by

$$P(E_X) = \exp\left(-\frac{d_1 m}{c\tau|\vec{p}|}\right) - \exp\left(-\frac{d_2 m}{c\tau|\vec{p}|}\right), \quad (50)$$

with $d_1 = 64$ m the distance from the beam dump to the front end of the detector, $d_2 = 87$ m the distance to the rear, and τ the X lifetime. The expressions for dN/dE_X found in Ref. [96] can be carried over directly to the pure axial case with the replacement $e\epsilon \rightarrow a_p$.⁵ Requiring

⁵ In the generalized Fermi-Williams-Weizäcker method used in Ref. [96] to derive the bounds, the Bremsstrahlung production cross-section for X is proportional to the cross-section for the Compton-like process $p + \gamma^* \rightarrow p + X$ (see e.g. Ref. [11] for a more detailed discussion). Upon inspecting the squared matrix element $|\mathcal{M}|^2$ for the $2 \rightarrow 2$ process in both the pure vector and axial vector case, and using the Dirac algebra and Dirac equation to commute the γ^5 factors, one finds that they are identical for both processes, with the replacement $e\epsilon \leftrightarrow a_p$.

N_{sig} to be smaller than the corresponding upper limit presented in Ref. [96] constrains the couplings a_p , g_e^V , and g_e^A . These bounds are shown in Fig. 4 and are generally found to be less stringent than other constraints on the relevant parameter space.

5.2.3 Comments on Other Constraints

The NA48/2 experiment [97] constrains the decay $\pi^0 \rightarrow \gamma X$, $X \rightarrow e^+e^-$. The amplitude for this process is proportional to the axial anomaly trace factor and vanishes for purely axial quark- X couplings, up to chiral-symmetry breaking effects proportional to light quark masses [25, 33, 98]. Note that this constraint required vector explanations of the ${}^8\text{Be}$ anomaly to be “protophobic”. This feature also implies that there are no strong constraints from pion decay constraints in proton beam dump experiments [99].

A related potential constraint comes from the KLOE-2 search for $\phi \rightarrow \eta X$, $X \rightarrow e^+e^-$, which depends specifically on the coupling of the light vector to the strange quark [100]. However, since the ϕ has $J^P = 1^-$ and the quark couplings of the light vector conserve parity, the argument for $\pi \rightarrow \gamma X$ can be applied here to the extent that the internal structure of the ϕ can be neglected. Even omitting this suppression, setting the axial form factor to be of the same order as the vector form factor we find that the bound imposed by this decay mode is subleading relative to the others considered in this section.

Other constraints on light vectors arise from atomic parity violation experiments [101] and limits on new particles from neutron-nucleus scattering [102]. Atomic parity violation does not give a bound in the present case since we consider an axial vector that conserves parity in the quark sector, but it would be relevant away from the purely axial (or vector) limit. Bounds from neutron-nucleus scattering are expected to be less important than in the vector case due to the decoherence induced by the coupling of X to nucleon spin rather than a conserved charge. Note as well that these constraints are already subdominant in the pure vector case.

6 A UV Completion for the ${}^8\text{Be}$ Anomaly

As we have seen, the constraints on a light vector boson can depend on both its lepton and quark couplings. In contrast, the ${}^8\text{Be}$ anomaly only specifies a range of quark couplings (provided the decay of the vector to electrons is fast enough). However, both the quark and lepton couplings of a light vector boson will typically be related to each other in an underlying UV complete theory. In this section, we construct a simple UV completion of a light vector with exclusively axial couplings to quarks that satisfies the basic assumptions listed at the beginning of Section 5. We also show that the theory can explain the Atomki ${}^8\text{Be}$ anomaly while maintaining consistency with existing experimental searches.

6.1 A Simple UV-Complete Theory

There has been recent interest in building UV-complete anomaly-free theories of light axially-coupled vector bosons [33, 103]. We will focus on the model presented in Sec. 5.2 of Ref. [33], and defer a more detailed model-building effort to a future investigation.

Consider a dark $U(1)_{\text{RH}}$ gauge theory with coupling g_D under which the right-handed SM fermions (e.g. u^c , d^c , e^c) are charged. Denote the corresponding charge of the RH SM fermion f^c as q_f . The charges are assumed to be the same for all three generations, with $q_d = q_e$ and the SM Higgs taken to be neutral under $U(1)_{\text{RH}}$. We include two dark Higgs fields, $H'_{u,d}$, both neutral under the SM gauge group and with $U(1)_{\text{RH}}$ charges $-q_u$, $-q_d$, respectively. The $U(1)_{\text{RH}}$ symmetry is spontaneously broken by non-zero vacuum expectation values for the dark Higgses, $v'_{u,d}$. In addition to the explicit charges, we allow for non-zero kinetic mixing ϵ between $U(1)_{\text{RH}}$ and $U(1)_Y$. This setup, detailed in Ref. [33], generically gives rise to mixed vector and axial couplings of the massive $U(1)_{\text{RH}}$ vector boson X to the charged Standard Model fermions (but not neutrinos).

In the scenario described above, the usual Standard Model Yukawa terms are forbidden by gauge invariance. Following Ref. [33], Yukawa interactions for the SM fermions can be generated by introducing a set of heavy new vector-like $SU(2)_L$ doublet fermions Ψ_f (and their conjugates, Ψ_f^c) with $U(1)_{\text{RH}}$ charges $-q_f$ and vector-like masses M (assumed to be the same for all Ψ for simplicity). The charges of Ψ_f under the SM gauge group are assumed to be the same as those of the corresponding left-handed SM fermion doublet. We can introduce the interactions

$$\begin{aligned} \mathcal{L}_{\text{Yukawa}}^{\text{UV}} = & -H'_u \Psi_u^c y'_u Q - H \Psi_u y_u u^c - H'_d \Psi_d^c y'_d Q - H^\dagger \Psi_d y_d d^c \\ & - H'_d \Psi_e^c y'_e L - H^\dagger \Psi_e y_e e^c + \text{h.c.} \end{aligned} \quad (51)$$

where $y'_{u,d,e}$ are generation-independent 3×3 matrices, $y_{u,d,e}$ are proportional to the corresponding Standard Model Yukawa matrices, and Q, L and H are the Standard Model quark, lepton, and Higgs doublets, respectively. Upon integrating out the vector-like fermions, these interactions yield effective SM-like Yukawa couplings of the form

$$\mathcal{L}_{\text{Yukawa}}^{\text{IR}} = y_{u,\text{eff}} H Q u^c + y_{d,\text{eff}} H^\dagger Q d^c + y_{e,\text{eff}} H^\dagger L e^c + \text{h.c.}, \quad (52)$$

where $y_{f,\text{eff}} \equiv y_f y'_f v'_{u,d}/M$. Note that M must be larger than about a TeV to avoid constraints from LHC searches on new vector-like quarks and leptons⁶. In this construction, we have assumed the framework of Minimal Flavor Violation (MFV), whereby Ψ_f transforms as a triplet under the corresponding $SU(3)_f$ flavor subgroup, and new contributions to flavor-changing neutral currents are suppressed.

⁶As discussed in Ref. [33], M cannot be arbitrarily large: obtaining the sizeable top quark Yukawa coupling for fixed values of the up-type axial coupling and m_X places an upper bound on M (assuming perturbatively small couplings in the matrices y, y'). However, we find that M can easily be in the multi-TeV range for $m_X \approx 17$ MeV, axial quark couplings $\lesssim 10^{-4}$, and $\sim \mathcal{O}(1)$ couplings in y, y' . We therefore expect the corresponding constraints to be readily satisfied in the parameter space relevant for explaining the ⁸Be anomaly.

Given the assumptions above, the couplings of the massive $U(1)_{\text{RH}}$ boson, X , to quarks are purely axial provided the following relation is satisfied:

$$g_D q_u \simeq -2g_D q_d \simeq \frac{4}{3} e \epsilon . \quad (53)$$

Matching to our previous notation, this implies

$$g_u = -2g_d, \quad g_{e,\mu}^A = g_d, \quad g_{e,\mu}^V = 2g_d \quad (54)$$

where g_d can be treated as a free parameter. As discussed in Ref. [33], demanding purely axial couplings to quarks requires a tuning of ϵ . Since our goal is simply to demonstrate that viable UV complete axial vector scenarios explaining the ^8Be anomaly exist, we will not comment further on this issue here.

As it stands, the would-be $U(1)_{\text{RH}}$ gauge symmetry is anomalous. This can be corrected by introducing additional fermions charged under $SU(3)_c$, $U(1)_Y$ and $U(1)_{\text{RH}}$ to cancel the anomalies. These new fermions, dubbed *anomalons* in Ref. [33], are vector-like under the SM gauge groups but chiral under $U(1)_{\text{RH}}$. They are assumed to obtain masses from the expectation values of the two dark Higgs fields, which will also contribute to the mass of the X vector boson. Since the anomalons carry color charge, their masses must be larger than about a TeV to be consistent with LHC searches. Demanding $m_X \simeq 17$ MeV then implies that [33]

$$\sqrt{(g_d)^2 + (g_u)^2} \lesssim \left(\frac{y_\psi}{4\pi} \right) \times 10^{-4} , \quad (55)$$

where y_ψ is the Yukawa coupling of the anomalon fermions to the dark Higgses, assumed to be the same for both up- and down-type species.

In this setup, the dark Higgs bosons are SM singlets and are weakly constrained, coupling to the visible sector either through the X vector boson, loops of the new vector-like fermions, or Higgs portal-type interactions. We therefore expect that there is enough freedom in the Higgs sector to straightforwardly satisfy the corresponding (highly model-dependent) constraints on the new Higgs scalars.

Note that the present construction could be modified to allow for $q_e \neq q_d$ by introducing another dark Higgs field. One could also envision a UV completion with generation-dependent couplings, along the lines discussed in Sec. 5.3 of Ref. [33], at the cost of additional tunings. Such modifications could potentially open up additional parameter space for explaining the ^8Be anomaly in terms of a light axially-coupled vector, but we do not pursue these directions further here.

6.2 Constraints on the Theory and the ^8Be Anomaly

Within this UV complete light axial vector scenario, we can now connect the quark couplings needed to address the ^8Be anomaly to the many constraints on the theory that also depend on lepton couplings. In Fig. 4 we show the most stringent bounds on the theory in the $|g_u|$ - $|g_d|$ plane with $g_u < 0$, $g_d > 0$, and the lepton couplings fixed in terms of g_d as in Eq. (54).

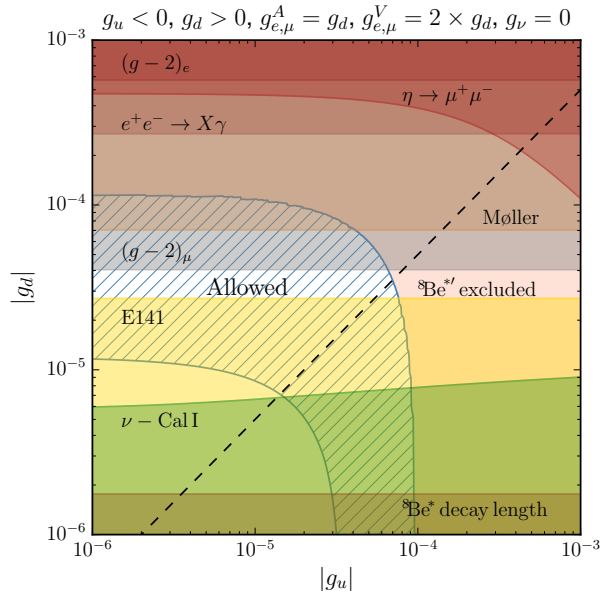


Figure 4: Quark level couplings required to explain the Atomki ${}^8\text{Be}$ anomaly along with the most important constraints in the UV complete scenario described in Section 6. For this specific model, g_u and g_d lie along the dashed black line. The experimentally allowed region is indicated as such, and includes values of the couplings consistent with an axial vector interpretation of the ${}^8\text{Be}$ anomaly, depicted by the hatched region.

Imposing the additional relation $g_u = -2g_d$ implied by the theory gives the dashed diagonal line. We do not include the *anomalon* bound of Eq. (55) in the figure as the coupling $y_\psi < 4\pi$ can be chosen such it does not constrain any additional parameter space. It would be beneficial to re-visit and sharpen this bound in a more detailed phenomenological study, however we defer this to future work. The hatched region in Fig. 4 indicates where the light vector can account for the Atomki ${}^8\text{Be}$ anomaly. This band was obtained by varying m_X , the nuclear matrix elements in Table 2, and the coefficients $\Delta u^{(p),(n)}$, $\Delta d^{(p),(n)}$, $\Delta s^{(p),(n)}$ in Eq. (17) across their allowed ranges, while also imposing the constraint of Eq. (40) on the ${}^8\text{Be}^{*'}$ transition rate. We see from this figure that there exists a small region of parameter space (with $|g_d| \sim 3 - 4 \times 10^{-5}$) in which the light axial vector provides a viable explanation of the ${}^8\text{Be}$ anomaly and is compatible with all other experimental constraints.

The strongest bounds on the theory tend to come from the lepton couplings of the light vector. Since these are fixed in terms of the quark couplings by our choice of UV completion, it is possible that there are other consistent UV models that are less constrained. Even more parameter space could open up if the assumptions about the couplings of the light vector listed at the start of Section 5 were relaxed. We postpone a more detailed investigation of these considerations to future work.

Let us also point out that the most important limit on the quark couplings alone comes from the Atomki measurements themselves [22], with the entire region to the upper right of the hatched region in Fig. 4 excluded by their data (up to nuclear uncertainties). Should

the anomaly disappear in the future with more data, these constraints would become even stronger. This again provides an important illustration of how precision nuclear measurements can be used to study light vectors (and other particles) beyond what is possible with other experiments.

7 Conclusions

Rare nuclear decays are a promising search channel for new hidden particle species with masses near the MeV scale. The anomaly seen in the e^+e^- spectrum of isoscalar ${}^8\text{Be}^*(1^+) \rightarrow {}^8\text{Be}(0^+)$ transitions at the Atomki facility can be explained by the emission of a light vector boson in this process [22, 24]. In this paper, we have studied such an interpretation for a light vector boson with axial couplings to quarks. To do so, we have performed a detailed *ab initio* calculation of the relevant nuclear transition matrix elements. We find that such a vector can account for the anomaly provided it has a mass of $m_X \simeq 17$ MeV and axial couplings to quarks on the order of $g_q \sim 10^{-5} - 10^{-4}$. Relative to vector bosons with exclusively vector couplings to quarks, the axial interpretation provides a natural suppression of vector emission in the isovector ${}^8\text{Be}^{*'}(1^+) \rightarrow {}^8\text{Be}(0^+)$ transition, where no anomaly is seen.

In this work we have also investigated other constraints on light vector bosons with axial quark couplings, and we have applied them to a simple UV realization of the theory. We find that the UV complete theory studied here can explain the ${}^8\text{Be}$ anomaly while being consistent with all current experimental searches. More generally, we also find that the Atomki measurements of the ${}^8\text{Be}$ system can provide the most sensitive model-independent probe of the interactions of a light vector with quarks. This motivates future searches for light vector bosons and other particles in rare nuclear transitions.

Acknowledgements

We thank Sonia Bacca, Angelo Calci, Barry Davids, Jonathan Feng, Susan Gardner, Yonatan Kahn, Richard Hill, Jason Holt, Saori Pastore, Achim Schwenk, Johannes Simonis, Tim Tait, Flip Tanedo, and Richard Woloshyn for helpful comments and discussions. SRS would also like to thank Angelo Calci and Johannes Simonis for providing the nuclear interactions used in this work. The IM-SRG code used in this work employs the Armadillo library [104]. Computations were performed with an allocation of computing resources at the Jlich Supercomputing Center. This work is supported by the Natural Sciences and Engineering Research Council of Canada (NSERC), with DM and SRS supported in part by Discovery Grants. TRIUMF receives federal funding via a contribution agreement with the National Research Council of Canada.

References

- [1] A. Leike, Phys. Rept. **317**, 143 (1999) doi:10.1016/S0370-1573(98)00133-1 [hep-ph/9805494].
- [2] P. Langacker, Rev. Mod. Phys. **81**, 1199 (2009) doi:10.1103/RevModPhys.81.1199 [arXiv:0801.1345 [hep-ph]].
- [3] M. Carena, A. Daleo, B. A. Dobrescu and T. M. P. Tait, Phys. Rev. D **70**, 093009 (2004) doi:10.1103/PhysRevD.70.093009 [hep-ph/0408098].
- [4] T. G. Rizzo, hep-ph/0610104.
- [5] M. Aaboud *et al.* [ATLAS Collaboration], Phys. Lett. B **761**, 372 (2016) doi:10.1016/j.physletb.2016.08.055 [arXiv:1607.03669 [hep-ex]].
- [6] V. Khachatryan *et al.* [CMS Collaboration], arXiv:1609.05391 [hep-ex].
- [7] J. Erler, P. Langacker, S. Munir and E. Rojas, JHEP **0908**, 017 (2009) doi:10.1088/1126-6708/2009/08/017 [arXiv:0906.2435 [hep-ph]].
- [8] N. Borodatchenkova, D. Choudhury and M. Drees, Phys. Rev. Lett. **96**, 141802 (2006) doi:10.1103/PhysRevLett.96.141802 [hep-ph/0510147].
- [9] P. Fayet, Phys. Rev. D **75**, 115017 (2007) doi:10.1103/PhysRevD.75.115017 [hep-ph/0702176 [HEP-PH]].
- [10] M. Pospelov, Phys. Rev. D **80**, 095002 (2009) doi:10.1103/PhysRevD.80.095002 [arXiv:0811.1030 [hep-ph]].
- [11] J. D. Bjorken, R. Essig, P. Schuster and N. Toro, Phys. Rev. D **80**, 075018 (2009) doi:10.1103/PhysRevD.80.075018 [arXiv:0906.0580 [hep-ph]].
- [12] B. Batell, M. Pospelov and A. Ritz, Phys. Rev. D **79**, 115008 (2009) doi:10.1103/PhysRevD.79.115008 [arXiv:0903.0363 [hep-ph]].
- [13] R. Essig, P. Schuster and N. Toro, Phys. Rev. D **80**, 015003 (2009) doi:10.1103/PhysRevD.80.015003 [arXiv:0903.3941 [hep-ph]].
- [14] M. Reece and L. T. Wang, JHEP **0907**, 051 (2009) doi:10.1088/1126-6708/2009/07/051 [arXiv:0904.1743 [hep-ph]].
- [15] R. Essig *et al.*, arXiv:1311.0029 [hep-ph].
- [16] J. Alexander *et al.*, arXiv:1608.08632 [hep-ph].
- [17] T. W. Donnelly, S. J. Freedman, R. S. Lytel, R. D. Peccei and M. Schwartz, Phys. Rev. D **18**, 1607 (1978). doi:10.1103/PhysRevD.18.1607

- [18] S. B. Treiman and F. Wilczek, Phys. Lett. B **74**, 381 (1978). doi:10.1016/0370-2693(78)90684-6
- [19] M. J. Savage, R. D. Mckeown, B. W. Filippone and L. W. Mitchell, Phys. Rev. Lett. **57**, 178 (1986). doi:10.1103/PhysRevLett.57.178
- [20] A. L. Hallin, F. P. Calaprice, R. W. Dunford and A. B. McDonald, Phys. Rev. Lett. **57**, 2105 (1986). doi:10.1103/PhysRevLett.57.2105
- [21] M. J. Savage, B. W. Filippone and L. W. Mitchell, Phys. Rev. D **37**, 1134 (1988). doi:10.1103/PhysRevD.37.1134
- [22] A. J. Krasznahorkay *et al.*, Phys. Rev. Lett. **116**, no. 4, 042501 (2016) doi:10.1103/PhysRevLett.116.042501 [arXiv:1504.01527 [nucl-ex]].
- [23] D. R. Tilley, J. H. Kelley, J. L. Godwin, D. J. Millener, J. E. Purcell, C. G. Sheu and H. R. Weller, Nucl. Phys. A **745**, 155 (2004). doi:10.1016/j.nuclphysa.2004.09.059
- [24] J. L. Feng, B. Fornal, I. Galon, S. Gardner, J. Smolinsky, T. M. P. Tait and P. Tanedo, Phys. Rev. Lett. **117**, no. 7, 071803 (2016) doi:10.1103/PhysRevLett.117.071803 [arXiv:1604.07411 [hep-ph]].
- [25] J. L. Feng, B. Fornal, I. Galon, S. Gardner, J. Smolinsky, T. M. P. Tait and P. Tanedo, Phys. Rev. D **95**, no. 3, 035017 (2017) doi:10.1103/PhysRevD.95.035017 [arXiv:1608.03591 [hep-ph]].
- [26] P. H. Gu and X. G. He, Nucl. Phys. B **919**, 209 (2017) doi:10.1016/j.nuclphysb.2017.03.023 [arXiv:1606.05171 [hep-ph]].
- [27] L. B. Chen, Y. Liang and C. F. Qiao, arXiv:1607.03970 [hep-ph].
- [28] Y. Liang, L. B. Chen and C. F. Qiao, arXiv:1607.08309 [hep-ph].
- [29] L. B. Jia and X. Q. Li, Eur. Phys. J. C **76**, no. 12, 706 (2016) doi:10.1140/epjc/s10052-016-4561-3 [arXiv:1608.05443 [hep-ph]].
- [30] T. Kitahara and Y. Yamamoto, Phys. Rev. D **95**, no. 1, 015008 (2017) doi:10.1103/PhysRevD.95.015008 [arXiv:1609.01605 [hep-ph]].
- [31] U. Ellwanger and S. Moretti, JHEP **1611**, 039 (2016) doi:10.1007/JHEP11(2016)039 [arXiv:1609.01669 [hep-ph]].
- [32] C. S. Chen, G. L. Lin, Y. H. Lin and F. Xu, arXiv:1609.07198 [hep-ph].
- [33] Y. Kahn, G. Krnjaic, S. Mishra-Sharma and T. M. P. Tait, JHEP **1705**, 002 (2017) doi:10.1007/JHEP05(2017)002 [arXiv:1609.09072 [hep-ph]].
- [34] O. Seto and T. Shimomura, arXiv:1610.08112 [hep-ph].
- [35] M. J. Neves and J. A. Helayël-Neto, arXiv:1611.07974 [hep-ph].

- [36] J. M. Blatt, V. F. Weisskopf, “Theoretical Nuclear Physics,” Springer-Verlag, 1979 (864pp).
- [37] J. D. Walecka, “Theoretical nuclear and subnuclear physics,” Oxford Stud. Nucl. Phys. **16**, 1 (1995).
- [38] J. Engel, S. Pittel and P. Vogel, Int. J. Mod. Phys. E **1**, 1 (1992). doi:10.1142/S0218301392000023
- [39] G. Jungman, M. Kamionkowski and K. Griest, Phys. Rept. **267**, 195 (1996) doi:10.1016/0370-1573(95)00058-5 [hep-ph/9506380].
- [40] J. Fan, M. Reece and L. T. Wang, JCAP **1011**, 042 (2010) doi:10.1088/1475-7516/2010/11/042 [arXiv:1008.1591 [hep-ph]].
- [41] A. L. Fitzpatrick, W. Haxton, E. Katz, N. Lubbers and Y. Xu, JCAP **1302**, 004 (2013) doi:10.1088/1475-7516/2013/02/004 [arXiv:1203.3542 [hep-ph]].
- [42] P. Agrawal, Z. Chacko, C. Kilic and R. K. Mishra, arXiv:1003.1912 [hep-ph].
- [43] J. Menendez, D. Gazit and A. Schwenk, Phys. Rev. D **86**, 103511 (2012) doi:10.1103/PhysRevD.86.103511 [arXiv:1208.1094 [astro-ph.CO]].
- [44] G. K. Mallot, Int. J. Mod. Phys. A **15S1**, 521 (2000) [eConf C **990809**, 521 (2000)] doi:10.1142/S0217751X00005309 [hep-ex/9912040].
- [45] J. R. Ellis, A. Ferstl and K. A. Olive, Phys. Lett. B **481**, 304 (2000) doi:10.1016/S0370-2693(00)00459-7 [hep-ph/0001005].
- [46] H. Y. Cheng and C. W. Chiang, JHEP **1207**, 009 (2012) doi:10.1007/JHEP07(2012)009 [arXiv:1202.1292 [hep-ph]].
- [47] G. S. Bali *et al.* [QCDSF Collaboration], Phys. Rev. Lett. **108**, 222001 (2012) doi:10.1103/PhysRevLett.108.222001 [arXiv:1112.3354 [hep-lat]].
- [48] M. Engelhardt, Phys. Rev. D **86**, 114510 (2012) doi:10.1103/PhysRevD.86.114510 [arXiv:1210.0025 [hep-lat]].
- [49] A. Abdel-Rehim, C. Alexandrou, M. Constantinou, V. Drach, K. Hadjiyiannakou, K. Jansen, G. Koutsou and A. Vaquero, Phys. Rev. D **89**, no. 3, 034501 (2014) doi:10.1103/PhysRevD.89.034501 [arXiv:1310.6339 [hep-lat]].
- [50] A. J. Chambers *et al.*, Phys. Rev. D **92**, no. 11, 114517 (2015) doi:10.1103/PhysRevD.92.114517 [arXiv:1508.06856 [hep-lat]].
- [51] J. Green *et al.*, arXiv:1703.06703 [hep-lat].
- [52] F. Bishara, J. Brod, B. Grinstein and J. Zupan, JCAP **02**, 009 (2017) doi:10.1088/1475-7516/2017/02/009 [arXiv:1611.00368 [hep-ph]].

- [53] K. Tsukiyama, S. K. Bogner, and A. Schwenk, Phys. Rev. Lett. **106**, 222502 (2011) doi:10.1103/PhysRevLett.106.222502 [arXiv:1006.3639 [nucl-th]]
- [54] H. Hergert, S. K. Bogner, T. D. Morris, A. Schwenk and K. Tsukiyama, Phys. Rept. **621**, 165 (2016) doi:10.1016/j.physrep.2015.12.007 [arXiv:1512.06956 [nucl-th]].
- [55] H. Hergert, arXiv:1607.06882 [nucl-th].
- [56] D. R. Entem and R. Machleidt, Phys. Rev. C **68**, 041001 (2003) doi:10.1103/PhysRevC.68.041001 [nucl-th/0304018].
- [57] P. Navrátil, Few Body Syst. **41**, 117 (2007) doi:10.1007/s00601-007-0193-3 [arXiv:0707.4680 [nucl-th]].
- [58] Doron Gazit, Sofia Quaglioni, and Petr Navrátil, Phys. Rev. Lett. **103**, 102502 (2009) doi:10.1103/PhysRevLett.103.102502 [nucl-th/0812.4444].
- [59] S. K. Bogner, R. J. Furnstahl and R. J. Perry, Phys. Rev. C **75**, 061001 (2007) doi:10.1103/PhysRevC.75.061001 [nucl-th/0611045].
- [60] R. Roth, A. Calci, J. Langhammer and S. Binder, Phys. Rev. C **90**, 024325 (2014) doi:10.1103/PhysRevC.90.024325 [arXiv:1311.3563 [nucl-th]].
- [61] Robert Roth, Sven Binder, Klaus Vobig, Angelo Calci, Joachim Langhammer, and Petr Navrátil Phys. Ref. Lett. **109**, 052501 (2012) doi:10.1103/PhysRevLett.109.052501 [arXiv:1112.0287 [nucl-th]].
- [62] H. Hergert, S. Binder, A. Calci, J. Langhammer, and R. Roth Phys. Rev. Lett. **110**, 242501 (2013) doi:10.1103/PhysRevLett.110.242501 [arXiv:1302.7294 [nucl-th]]
- [63] Sven Binder, Joachim Langhammer, Angelo Calci, and Robert Roth Phys. Lett. B **736**, 119 (2014) doi:10.1016/j.physletb.2014.07.010 [arXiv:1312.5685 [nucl-th]]
- [64] V. Somà, A. Cipollone, C. Barbieri, P. Navrtil, and T. Duguet Phys. Rev. C **89**, 061301(R) (2014) doi:10.1103/PhysRevC.89.061301 [arXiv:1312.2068 [nucl-th]]
- [65] G. R. Jansen, J. Engel, G. Hagen, P. Navrátil, and A. Signoracci Phys. Rev. Lett. **113**, 142502 (2014) doi:10.1103/PhysRevLett.113.142502 [arXiv:1402.2563 [nucl-th]]
- [66] S. K. Bogner, H. Hergert, J. D. Holt, A. Schwenk, S. Binder, A. Calci, J. Langhammer and R. Roth, Phys. Rev. Lett. **113**, 142501 (2014) doi:10.1103/PhysRevLett.113.142501 [arXiv:1402.1407 [nucl-th]].
- [67] K. Hebeler, S. K. Bogner, R. J. Furnstahl, A. Nogga and A. Schwenk, Phys. Rev. C **83**, 031301 (2011) doi:10.1103/PhysRevC.83.031301 [arXiv:1012.3381 [nucl-th]].
- [68] C. Drischler, K. Hebeler, and A. Schwenk Phys. Rev. C **93**, 054314 (2016) doi:10.1103/PhysRevC.93.011302, [arXiv:1510.06728 [nucl-th]].

- [69] J. Simonis, K. Hebeler, J. D. Holt, J. Menéndez, and A. Schwenk, Phys. Rev. C **93**, 011302 (2016) doi:10.1103/PhysRevC.93.011302, [arXiv:1508.05040 [nucl-th]].
- [70] G. Hagen *et al.*, Nature Phys. **12**, no. 2, 186 (2015) doi:10.1038/nphys3529 [arXiv:1509.07169 [nucl-th]].
- [71] R. F. Garcia Ruiz *et al.*, Nature Phys. **12**, 594598 (2016) doi:10.1038/nphys3645 [arXiv:1602.07906 [nucl-ex]].
- [72] G. Hagen, G. R. Jansen, and T. Papenbrock, Phys. Rev. Lett. **117**, 172501 (2016) doi:10.1103/PhysRevLett.117.172501 [arXiv:1605.01477 [nucl-th]].
- [73] S. R. Stroberg, A. Calci, H. Hergert, J. D. Holt, S. K. Bogner, R. Roth and A. Schwenk, Phys. Rev. Lett. **118**, no. 3, 032502 (2017) doi:10.1103/PhysRevLett.118.032502 [arXiv:1607.03229 [nucl-th]].
- [74] E. Gebrerufael, A. Calci and R. Roth, Phys. Rev. C **93**, no. 3, 031301 (2016) doi:10.1103/PhysRevC.93.031301 [arXiv:1511.01857 [nucl-th]].
- [75] K. Tsukiyama, S. K. Bogner, and A. Schwenk, Phys. Rev. C **85**, 061304(R) (2012) doi:10.1103/PhysRevC.85.061304 [arXiv:1203.2515 [nucl-th]]
- [76] T. D. Morris, N. Parzuchowski and S. K. Bogner, Phys. Rev. C **92**, no. 3, 034331 (2015) doi:10.1103/PhysRevC.92.034331 [arXiv:1507.06725 [nucl-th]].
- [77] Steven R. White, J. Chem. Phys. **117**, 7472 (2002) doi:10.1063/1.1508370
- [78] B. A. Brown, and W. D. M. Rae, Nucl. Data Sheets **120**, 115 (2014) doi:10.1016/j.nds.2014.07.022
- [79] N. Parzuchowski, S. R. Stroberg, H. Hergert, P. Navrátil, and S. K. Bogner, in prep.; N. Parzuchowski Ph.D. thesis, Michigan State University (2017).
- [80] J. Eisenberg and W. Greiner, “Excitation Mechanism of the Nucleus” North Holland Publishing Co. (1970)
- [81] A. Calci and R. Roth, Phys. Rev. C **94**, no. 1, 014322 (2016) doi:10.1103/PhysRevC.94.014322 [arXiv:1601.07209 [nucl-th]].
- [82] S. Pastore, R. B. Wiringa, S. C. Pieper and R. Schiavilla, Phys. Rev. C **90**, no. 2, 024321 (2014) doi:10.1103/PhysRevC.90.024321 [arXiv:1406.2343 [nucl-th]].
- [83] J. Menéndez, D. Gazit, and A. Schwenk, Phys. Rev. D **86**, 103511 (2012) doi:10.1103/PhysRevD.86.103511 [http://link.aps.org/doi/10.1103/PhysRevD.86.103511].
- [84] F. C. Barker, Nucl. Phys. A **83** 418 (1966).
- [85] J. Gulyas *et al.*, Nucl. Instrum. Meth. A **808**, 21 (2016) doi:10.1016/j.nima.2015.11.009 [arXiv:1504.00489 [nucl-ex]].

- [86] G. Bellini *et al.*, Phys. Rev. Lett. **107**, 141302 (2011) doi:10.1103/PhysRevLett.107.141302 [arXiv:1104.1816 [hep-ex]].
- [87] M. Deniz *et al.* [TEXONO Collaboration], Phys. Rev. D **81**, 072001 (2010) doi:10.1103/PhysRevD.81.072001 [arXiv:0911.1597 [hep-ex]].
- [88] P. Vilain *et al.* [CHARM-II Collaboration], Phys. Lett. B **335**, 246 (1994). doi:10.1016/0370-2693(94)91421-4
- [89] G. W. Bennett *et al.* [Muon g-2 Collaboration], Phys. Rev. D **73**, 072003 (2006) doi:10.1103/PhysRevD.73.072003 [hep-ex/0602035].
- [90] T. Blum, A. Denig, I. Logashenko, E. de Rafael, B. Lee Roberts, T. Teubner and G. Venanzoni, arXiv:1311.2198 [hep-ph].
- [91] G. F. Giudice, P. Paradisi and M. Passera, JHEP **1211**, 113 (2012) doi:10.1007/JHEP11(2012)113 [arXiv:1208.6583 [hep-ph]].
- [92] E. M. Riordan *et al.*, Phys. Rev. Lett. **59**, 755 (1987). doi:10.1103/PhysRevLett.59.755
- [93] J. P. Lees *et al.* [BaBar Collaboration], Phys. Rev. Lett. **113**, no. 20, 201801 (2014) doi:10.1103/PhysRevLett.113.201801 [arXiv:1406.2980 [hep-ex]].
- [94] P. L. Anthony *et al.* [SLAC E158 Collaboration], Phys. Rev. Lett. **95**, 081601 (2005) doi:10.1103/PhysRevLett.95.081601 [hep-ex/0504049].
- [95] P. Masjuan and P. Sanchez-Puertas, JHEP **1608**, 108 (2016) doi:10.1007/JHEP08(2016)108 [arXiv:1512.09292 [hep-ph]].
- [96] J. Blumlein and J. Brunner, Phys. Lett. B **731**, 320 (2014) doi:10.1016/j.physletb.2014.02.029 [arXiv:1311.3870 [hep-ph]].
- [97] J. R. Batley *et al.* [NA48/2 Collaboration], Phys. Lett. B **746**, 178 (2015) doi:10.1016/j.physletb.2015.04.068 [arXiv:1504.00607 [hep-ex]].
- [98] H. Georgi, “Weak Interactions and Modern Particle Theory,” Menlo Park, Usa: Benjamin/cummings (1984) 165p
- [99] J. Blumlein and J. Brunner, Phys. Lett. B **701**, 155 (2011) doi:10.1016/j.physletb.2011.05.046 [arXiv:1104.2747 [hep-ex]].
- [100] D. Babusci *et al.* [KLOE-2 Collaboration], Phys. Lett. B **720**, 111 (2013) doi:10.1016/j.physletb.2013.01.067 [arXiv:1210.3927 [hep-ex]].
- [101] S. G. Porsev, K. Beloy and A. Derevianko, Phys. Rev. Lett. **102**, 181601 (2009) doi:10.1103/PhysRevLett.102.181601 [arXiv:0902.0335 [hep-ph]].
- [102] R. Barbieri and T. E. O. Ericson, Phys. Lett. **57B**, 270 (1975). doi:10.1016/0370-2693(75)90073-8

[103] A. Ismail, W. Y. Keung, K. H. Tsao and J. Unwin, Nucl. Phys. B **918**, 220 (2017)
doi:10.1016/j.nuclphysb.2017.03.001 [arXiv:1609.02188 [hep-ph]].

[104] C. Sanderson, Technical Report, NICTA 2010[http://arma.sourceforge.net/armadillo_nicta_2010.pdf]